Experimental Investigation into the Aerodynamic and Aeroacoustic Performance of Bioinspired Small-Scale Propeller Planforms

Foad Moslem
Experimental Aerodynamic and Aeroacoustic Laboratory, Faculty of New Sciences and Technologies, University of Tehran, North Kargar Street, Tehran, 14395-1561, Iran
E-mail: foad.moslem@ut.ac.ir

Mehran Masdari[1]
Assistant Professor
Experimental Aerodynamic and Aeroacoustic Laboratory, Faculty of New Sciences and Technologies, University of Tehran, North Kargar Street, Tehran, 14395-1561, Iran
E-mail: m.masdari@ut.ac.ir

Kirchu Fedir
Associate Professor
Aviation Engines Department, National Aviation University, Liubomyra Huzara Ave, Kyiv, 03058, Ukraine
E-mail: fkirchu@nau.edu.ua

Behzad Moslem
Faculty of Industrial Engineering, Islamic Azad University Science and Research Branch, Tehran, Iran
E-mail: behzad.moslem@srbiau.ac.ir

[1] Corresponding author. m.masdari@ut.ac.ir

Abstract

The multi-rotors have a limited operational period and generate too much noise, which is insufficient for complex tasks and adversely affects humans' and animals' health. Nevertheless, their market has become increasingly popular. Therefore, low-noise products are more competitive, and aerodynamic and acoustic improvements are critical. This investigation aims to design a small bioinspired propeller with the same power input as a conventional propeller to achieve the same or better aerodynamic performance while decreasing noise. Accordingly, an experimental investigated the impacts of operation conditions and varied geometric parameters on six small propellers' aeroacoustic performances with a unique planform shape inspired by five insects and one plant, such as Blattodea, Hemiptera, Hymenoptera, Neuroptera, Odonata, and Maple Seed. Each propeller was operated at eleven rotational speeds ranging from 3000 to 8000 RPM with no freestream velocity for simulating hover conditions. Compared to the baseline propeller, the results demonstrate that all bioinspired propellers produce more thrust for the same power supply, reduce harmonic and broadband noise, and provide a better noise level. Also, their rotational speed is lower and their figure of merit is higher than the baseline propeller at hover flight with 3N thrust. They all outperform the baseline propeller in terms of hover efficiency at all thrust values considered. Besides, the Neuroptera propeller is more efficient than other propellers, and decreasing 5.5W of power and reducing 7.9 dBA at hover flight with 3N thrust and 1.5 meters distance, compared to the baseline propeller.

Keywords:

Aeroacoustics, Aerodynamic Performance, Propeller, Insect Bioinspiration, Planform

Graphical Abstract

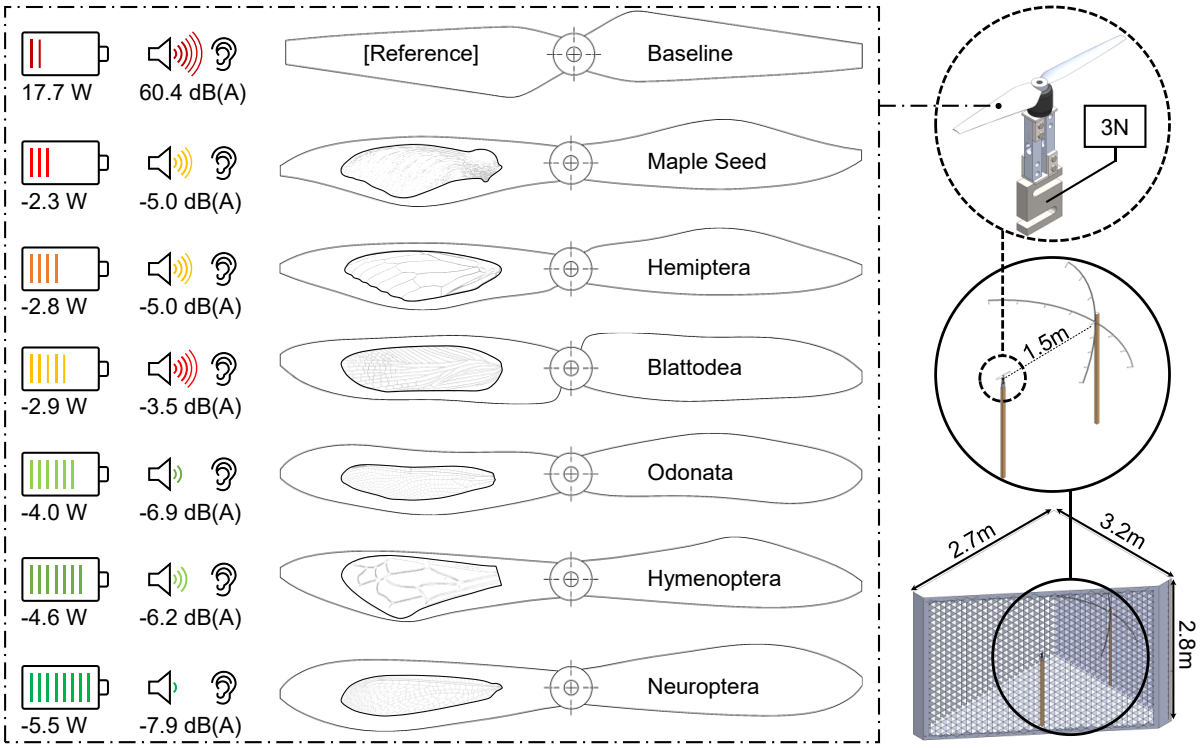

NOMENCLATURE

A	Propeller disk area (m^2)	p_{ref}	Reference pressure, 2×10^{-5} Pa
C_Q	Coefficient of torque	Q	Torque (N. m)
C_T	Coefficient of thrust	R	Propeller radius (m)
dB	Decibel	SPL_A	A-weighted sound pressure level
dBA	A-weighted decibel	RPM	Revolutions per minute
FoM	Figure of merit	$sUAS$	Small Unmanned Aerial Systems
$OASPL$	Overall A-weighted sound pressure level	T	Thrust (N)
P_m	Mechanical power	$UASs$	Unmanned Aerial Systems
PL	Power loading	ρ	Flow density (kg/m^3)
p_A	Instantaneous sound pressure measured using the standard frequency weighting A	Ω	Propeller rotational speed (rev/sec)

1. INTRODUCTION

The Unmanned Aerial Systems (UASs) market has become increasingly popular for commercial, recreational, and scientific research applications in recent years, due to their small size, low-cost electronic devices, hovering and maneuvering ability, ability to perform difficult or dangerous tasks, and user-friendly flight controllability. Various UAS systems have been presented as a new means of transportation and delivery over distances ranging from 1 to 300 km. Small Unmanned Aerial Systems (sUAS) have offered promising solutions for various civilian applications, such as food and postal package delivery, medical supplies delivery, surveillance, rescue operations, reaching hard-to-reach areas, inspecting buildings, mapping construction, traffic control, aerial photography, video recording, agriculture, and entertainment. Nowadays, multi-rotors are the preferred sUAS platform, and their presence has been increased. Currently, multi-rotors have an operational period of less than one hour, which is insufficient for complex tasks. Besides, the noise generated from the operating multi-rotors is another essential problem that can be limited to their use. Noise has adverse effects on humans' and animals' health, such as fatigue, mental illness, cognitive dysfunction, aggression, hormonal disorders, stress, stroke, heart attack, hypertension, diabetes, sleep disruption, and hearing impairment [1]. Therefore, low-noise products are more competitive in the market, and aerodynamic and acoustic improvements are critical to increasing operational duration and lowering noise.

The two primary noise sources of multi-rotors are the propellers and the motors. The propellers are the main source of lift generation and the predominant noise heard during flight phases under normal conditions, so in comparison, the noise of the motors can be ignored [2]. The propellers introduce complicated aerodynamic and aeroacoustic interactions that understanding their characteristics is critical for more efficient and quiet design. Figure 1 shows aerodynamic noise sources. Small propellers are operated at lower Reynolds number regimes ($10^4 - 10^5$) and by decreasing the Reynolds number in this range, the lift decreases, whereas the drag increases. Propellers only have a few aerodynamic noise sources due to their size and Reynolds number regimes. A single propeller blade's noise mechanisms contribute to two main classes: broadband noise and harmonic noise. Harmonic noise includes thickness noise, loading noise, and blade-vortex interactions. Thickness noise is caused by the fluid being displaced around the blade as it turns and being directed towards the propeller plane. Loading noise is generated predominantly above and below the propeller plane due to the surface's steady and unsteady pressure loads. When the Mach number is less than one, the loading noise outweighs the harmonic noise. However, blade-vortex interaction (BVI) noise is heard when the previously generated tip vortices and entrance blade collision. Broadband noise contains inflow turbulence and vortex noise. Inflow turbulence is present in broadband noise, and vortex noise is produced by the interaction of the flow with various components of the blade, such as the leading edge, trailing edge, blade-tip, or turbulent flow in the wake.

There have been various noise reduction approaches to changing the design of the propeller blade, but these techniques must have no profound impact on aerodynamic performance and vehicle flight dynamics. Propeller noise studies, especially for larger vehicles like helicopters, focus on harmonic and impulsive noise sources. However, isolated small-scale propellers suffer from a different type of noise [3]. Tonal noise in the low to mid-frequency region dominates isolated small-scale propellers, as it does full-scale propellers [4]. Broadband noise is substantial for small propellers at higher frequencies [5], [6]. In recent years, some experimental and numerical research has been done to understand and improve the aerodynamic performance and aeroacoustic signatures of small propellers in different flight modes and conditions, such as hover flight, forward flight, and flight in harsh environments. Hovering quadrotors' noise signatures can be considerably decreased by replacing them with customized propellers. Zawodny and Boyd [7] studied hover acoustic measurements of isolated small propeller-airframe interactions. According to the analysis, under certain propeller tip clearance circumstances, the presence of the airframe surfaces might cause noise levels similar to or larger than the propeller blade surfaces. Whelchel, Alexander, and Intaratep [8] experimentally investigated the noise and thrust produced by four small propellers operating at takeoff conditions and propeller-airframe interaction and compared them with a DJI Matrice 600 Pro propeller. Brandt and Selig [9] tested 79 small propellers fitted in the 9- to 11-in diameter that operate in the low Reynolds number range of 50,000 to 100,000 to quantify propeller efficiency. Propeller efficiencies range from a high of 0.65 (for an efficient propeller) to a low of 0.28 (for an efficient propeller). According to the findings, appropriate propeller selection for UAVs can have a significant impact on aircraft performance. Wisniewski *et al.* [10] analyzed thrust, sound pressure level (SPL), and RPM data from a DJI standard propeller and three custom-designed propellers at 1.4 lbf thrust. They realized the noise signature of hovering quadcopters can be significantly reduced by replacing them with custom-designed, wide chord multi-bladed propellers. McKay and Kingan [11] observed that the minor variations in the small propeller's RPM produced unsteady loading and thickness noise, and after that, blade passing frequency tones started showing up. Zawodny and Haskin [12] performed a subsequent detailed experimental investigation which showed how the relative importance of thickness and loading noise changed with observer position and how interference between the two noise sources could be important at specific locations. Andria *et al.* [13] presented a way to improve small propeller performance. The modeling of the propeller's blades and hub, followed by simulation to estimate thrust, was the first step in this procedure. Finally, the thrust produced by different propellers was compared to better understand the changes that may be made. The aeroacoustic fingerprints of two small propellers were studied experimentally by Sinibaldi and Marino [14]. They observed that the improved propeller produces significantly less noise than the standard propeller at lower thrust settings.

Active and passive flow control techniques can be utilized to increase propeller performance and minimize noise. Active flow control methods are unviable for small propellers. On the other hand, passive flow control approaches manipulate the boundary

layer without using any extra energy. Because flying animals have evolved over millions of years to create efficient, high-performance wings, nature is an excellent source for passive flow control approaches for designing bioinspired wings. Yang, Wang, *et al.* [15] adopted an owl wing-inspired trailing-edge serrations for noise reduction of a small propeller and compared its aerodynamic and acoustic performance with a baseline propeller in the forward flight condition. Cambray *et al.* [16] investigated the noise production process from small propellers as well as the influence of trailing-edge serrations on noise reduction in their tests. Ning, Wlezien, and Hu [17] studied the noise attenuation capability of three distinct bio-inspired saw-tooth serrations applied to the baseline propeller to assess the serration's noise attenuation potential on a small propeller. To achieve maximal noise reduction while preserving aerodynamic power, Xiong, Nguyen, and Cramer [18] optimized an anti-phase alternating trailing-edge pattern for propeller noise suppression. Yang, Liu, Hu, *et al.* [19] presented a small wavy propeller and compared its aerodynamic and acoustic performance with a baseline propeller. Hintz *et al.* [20] presented experimental research findings to determine the influence of a bio-inspired blade planform on small-scale propeller thrust and energy consumption. Ning and Hu [21] examined a small propeller's aerodynamic and aeroacoustic properties with a novel planform shape inspired by the maple seed by comparing it to a typical baseline propeller in hover flight. They showed that the bioinspired propeller could provide equivalent thrust with constant power input while emitting less noise.

The goal of this research is to create a small bioinspired propeller that has the same power input as a conventional propeller and can achieve the same or better aerodynamic performance while reducing noise. Nature appears to have done an incredible job of designing insects' wings that are both practical and capable of sustained flight. Insects have different species, fly slower than birds, and operate at low Reynolds number flows. They take advantage of vortex patterns to provide the additional lift they require to fly [22]. Several studies have connected flow separation and vortex generation to insect flight's high lift aerodynamics [23]. The tip vortex adds significantly to the lift generated by a flat plate with an aspect ratio and motion amplitudes equal to those seen in nature, according to experimental studies [24]. Ning and Hu [21] showed that the majority of the thrust for a rotary-wing is known to be created between 50% and 90% of the propeller radius, and at Reynolds numbers ranging from 10,000 to 100,000, the lift to drag ratio dramatically increases as the Reynolds number increases. As shown in Fig. 2, these bioinspired wing planforms appear to be more compatible with the lift distribution, where the largest chord length is in the high lift area. As a result, if these planform configurations are used in the design, the propeller will operate at a better lift to drag ratio. Accordingly, an experimental test is mainly used to study six small propellers' aerodynamic and aeroacoustic performance with unique planform shapes inspired by five insects and one plant, such as Blattodea, Hemiptera, Hymenoptera, Neuroptera, Odonata, and Maple Seed. For the current investigation's comparison study, a typical tapered small-scale propeller was used as the baseline propeller.

2. Experimental Setup

The experiments were performed in the Experimental Aerodynamics and Aeroacoustics Research Laboratory's anechoic chamber at the University of Tehran. A schematic of the facility is sketched out in Fig. 3. The inner dimensions of the anechoic chamber from wedge tip to wedge tip are 3m long, 2.5m wide, and 2.56m tall with a low-frequency cut-off of 100 Hz. To reduce noise contamination, the propeller noise and loadings at the hover flight condition were measured using an external PC and DAQ.

Our experimental analysis compares the aeroacoustic features of seven propellers with different planforms. We call the first one the baseline propeller and the others the Blattodea, Hemiptera, Hymenoptera, Maple Seed, Neuroptera, and Odonata propellers, respectively. The shape of the baseline propeller is derived from a two-bladed 9450 model for the DJI Phantom II that has a 9.4" diameter and a pitch of 5.0", which is a small-scale commercial drone propeller used for video shooting and entertainment. The Blattodea propeller's shape is inspired by a type of insect divided into approximately 4400 species of beetles and 3000 species of termites. The Hemiptera propeller's shape is inspired by a type of insect with about 50 to 80 thousand species, including cicadas. Their flying abilities are well developed for short distances and sporadically. The Hymenoptera propeller's shape is inspired by one of the largest insect groups with more than 150,000 species, including bees. Their flight distance varies from small to large depending on the species size, and they typically have two pairs of wings. The Maple Seed propeller's shape is inspired by a thin, smooth wing with dry fibrous tissue attached to the nut of maple tree seeds. Due to the grain weight relative to the whole structure, the seeds rotate like a helicopter's propeller when they fall. The Neuroptera propeller's shape is inspired by a type of insect with two pairs of membranous wings and consists of about 6,000 species. Finally, The Odonata propeller's shape is inspired by a type of insect with two long, transparent wings that move independently. They fly straight, and the flight muscles are attached directly to the wings.

Based on Ning and Hu [21], the chord length from the largest chord on the planform to the propeller's tip decreased linearly. It was calculated by $C_r = C_{tip}/r$, where C_r is the chord length at the corresponding radius location, and r represents a non-dimensional radial distance. The blade twisted 17.7 degrees at the largest chord on the planform to 4.7 degrees at the propeller's tip. Like Ning and Hu [21], due to a strength worry, we reshaped every single profile with a doubled thickness E63 airfoil based on the camber line and rescaled the diameter to 24cm fixed for both propellers, and our developed propellers achieved 0.12 solidity like other ordinary small propellers. The schematic and geometric details of all propellers are shown in Fig. 4. The propellers with a 0.1mm airfoil trailing edge thickness were manufactured using the Umbreil3d 3D printer with a 100μm resolution and a density of 20%, and were made by PLA material.

The experimental setup is shown in Fig. 3, which measures the thrust, torque, RPM, and sound pressure level. The testing equipment was positioned on a lab stand 6.25D above the surface such that the thrust was directed toward the chamber floor. When the propeller is in hover mode, the entire rig experiences nearly no vibration. For the measurement of the propeller thrust and torque, driven by an AIR 2213 electric brushless Tiger Motor with 920 KV, a three-component balance (a 30kg force capacity AmCells S-type and two 5kg force capacity YZC-133 loadcell) produced by the Experimental Aerodynamics and Aeroacoustics Research Group was located directly below the motor. An Agilent E3621A DC power supply provided power to the motor set at a constant 11.1 V for all tests. The propeller rotational speed was regulated using a T-Motor 20A AIR electronic speed controller, which received time pulse signals from an Arduino Uno and measured using a LUTRON DT-2268 tachometer. The T9545 propeller was tested to validate the aerodynamic facility's accuracy, and the results were compared to its datasheet, which showed the error was about 0.8%.

The microphone array is shown in Fig. 3. All acoustic measurements were made using fifteen 1/2 inch free-field Bruel & Kjaer microphones type 4190 microphones. The microphones were configured on two crossed C-shaped arrays at a 6.25D (1.5 meters) radial distance from the center of the propeller and were positioned every 15° between 0° and 45° and every 7.5° between 0° and -30° on the roll-plane C-shape array configuration and every 13° on the propeller plane from the common microphone. The goal of this microphone array is to demonstrate noise reduction directivity and provide more accurate results than a single microphone. Wind-screens covered the microphones, and the frame was lined with absorbing material to reduce reflections. They were individually calibrated using a B&K Type 4231 sound calibrator. The calibrator showed ±0.2 dB calibration accuracy. The microphone's measurement uncertainty was ±1 dB up to 20 kHz. Noise measurements were performed on all microphones, but only results for microphone number five are reported for the sake of compactness. While acoustic pressure was recorded for 15 seconds at a sampling rate of 48 kHz, only the last 5 seconds of data was used to calculate the acoustic spectra. This time range was selected to consider only the steady-state noise. The thrust, torque, and rotation rates were recorded synchronously with the acoustic data. The balance data was collected for 5 seconds at a sampling rate of 2000 Hz. The thrust, torque, RPM, and microphone data were recorded using a LAN-XI DAQ data acquisition system and collected by an in-house developed data acquisition and control. For each Fourier transform, the recorded acoustic data was divided into time blocks of 1024 samples. Hanning windows were used, with a 50 percent overlap.

While investigating the impacts of propeller operation conditions and varied geometric parameters on aerodynamic loads and noise emissions, each propeller was operated at eleven rotational speeds ranging from 3000 rpm to 8000 rpm in 500 rpm increments. This rotation rate represents the typical RPM for small drones. Also, the freestream velocity was 0 m/s because the propeller was operated at a simulated hover

condition. Representative values of local chord-based Reynolds and Mach numbers are displayed in Table 1.

Before testing in place, the load cells were calibrated by applying known weights to provide steady thrust and torque loads along the axis of each load cell, which covers the range of propeller loadings, and the calibration was verified before each set of tests. The thrust and torque measurement uncertainties were obtained at about 0.29% and 0.15% of the full range. The repeatability of 20 measurements on the baseline model at 3000, 5500, and 8000 RPM was used to calculate the uncertainty of the microphone data. The uncertainties for the total noise's overall A-weighted sound pressure level (OASPL) were obtained at about 0.1 dB and 0.9 dB, respectively. The rotational speed uncertainty is 5 RPM, which can be ignored.

3. Results and Discussion

This section presents and discusses the contribution of a bioinspired planform to modifying small propeller aerodynamic efficiency and acoustic signature in three parts. In the first part, experimental aerodynamic performance is presented, and efficiency is studied, in the second part, the experimental acoustic signature is investigated and noise reduction is discussed, and in the last part aeroacoustic results compared to the T9545 propeller.

3.1. Aerodynamic Performance Results

The payload and endurance duration of multi-rotors are determined by aerodynamic performance. To characterize the designed propellers' performance, the coefficient of thrust (C_T), coefficient of torque (C_Q), mechanical power (P_m), and figure of merit (FoM) have been calculated, as shown in Equations (1), (2), (3), and (4) respectively, where ρ is flow density (kg/m^3), A is the propeller disk area (m^2), Ω is propeller rotational speed (rev/sec), R is propeller radius (m), T is thrust (N), and Q is torque ($N.m$). Also, the parameter of power loading (PL) is defined as the available thrust for a given power in order to measure the efficiency of the rotors and is demonstrated by Equation (5). We utilize both dimensional and non-dimensional data in propeller comparison, and there is no obligation to use just non-dimensional data. Furthermore, the sound pressure level is affected by the propeller's dimensional loading.

$$C_T = \frac{T}{\rho A \Omega^2 R^2} \tag{1}$$

$$C_Q = \frac{Q}{\rho A \Omega^2 R^3} \tag{2}$$

$$P_m = Q \cdot (2\pi \cdot \frac{RPM}{60}) \tag{3}$$

$$FoM = \frac{C_T^{3/2}/\sqrt{2}}{C_Q} \quad (4)$$

$$PL = T/P \quad (5)$$

Figure 5 and 6 presents the comparative aerodynamic results. When the rotational speed increase from 3000 RPM to 8000 RPM, the time-averaged thrust increase for the baseline propeller from 0.51N to 3.82N, for the Blattodea propeller from 0.72N to 5.17N, for Hemiptera propeller from 0.85N to 4.86N, for Hymenoptera propeller from 1.02N to 5.77N, for Maple Seed propeller from 0.74N to 5.04N, for Neuroptera propeller from 1.11N to 7.03N, and for Odonata propeller from 0.83N to 6.01N.

Also, when the rotational speed increase from 3000 RPM to 8000 RPM, the power loading of the baseline increase from 0.07 N/W to 0.19 N/W, the Blattodea increase from 0.10 N/W to 0.26 N/W, the Hemiptera increase from 0.11 N/W to 0.24 N/W, the Hymenoptera increase from 0.14 N/W to 0.29 N/W, the Maple Seed increase from 0.10 N/W to 0.25 N/W, the Neuroptera increase from 0.15 N/W to 0.35 N/W, and the Odonata increase from 0.11 N/W to 0.30 N/W. Therefore, the power loading of the bioinspired-planform propellers in all RPM and thrust ranges are higher than the baseline propeller.

At hover flight with 3N thrust, the rotational speed of the Neuroptera propeller is 4860 RPM, the Hymenoptera propeller is 5200 RPM, the Odonata propeller is 5460 RPM, the Blattodea propeller is 5915 RPM, the Hemiptera propeller is 5925 RPM, the Maple Seed propeller is 6120 RPM, and the baseline propeller is 7060 RPM. The results show that Neuroptera is 36.6 %, Hymenoptera is 31.0 %, Odonata is 26.7 %, Blattodea is 19.1 %, Hemiptera is 18.9 %, and Maple Seed is 15.7 % slower than the baseline propeller at the same thrust. The drop in rotational speed shows that the thrust coefficient of the bioinspired propellers is greater than that of the baseline propeller.

Further, at hover flight with 3N thrust, the required time-averaged power of the Neuroptera propeller is 12.2W, the Hymenoptera propeller is 13W, the Odonata propeller is 13.7W, the Blattodea and Hemiptera propellers are 14.8W, the Maple Seed propeller is 15.3W, and the baseline propeller is 17.7W. The results indicate that the Neuroptera propeller consumes 5.5W, the Hymenoptera propeller consumes 4.6W, the Odonata propeller consumes 4.0W, the Blattodea and Hemiptera propellers consume 2.9W, and the Maple Seed propeller consumes 2.3W less power than the baseline propeller at hover flight, and with a maximum power decrease of 31.0% in Neuroptera propeller, 26.2% in Hymenoptera propeller, 22.6% in Odonata propeller, 16.2% in Blattodea and Hemiptera propeller, and 13.3% in Maple Seed propeller, the bioinspired propellers perform better than the baseline propeller. In conclusion, at hover flight with 3N thrust, the power loading of the Neuroptera propeller is 0.25 N/W, the Hymenoptera propeller is 0.23 N/W, the Odonata propeller is 0.22 N/W, the Blattodea, Hemiptera, and Maple Seed propellers are 0.20 N/W, and the baseline propeller is 0.17 N/W.

Furthermore, at hover flight with 3N thrust, the figure of merit of the Neuroptera propeller is 4.06, the Hymenoptera propeller is 3.79, the Odonata propeller is 3.52, the Hemiptera propeller is 3.34, the Blattodea propeller is 3.30, the Maple Seed propeller is 3.20, and the baseline propeller is 2.79. At this thrust, the figure of merit of the Neuroptera propeller is about 45.5%, the Hymenoptera propeller is about 35.7%, the Odonata propeller is about 25.9%, the Hemiptera propeller is about 19.5%, the Blattodea propeller is about 18.1%, and the Maple Seed propeller is about 14.5% higher than the baseline propeller, which leads to less torque or more thrust.

The results demonstrate that the bioinspired propellers produce more thrust than the baseline propeller for the same power supply and generate less drag than the baseline propeller at hover flight with 3N thrust. At all thrust numbers evaluated, the bioinspired propellers exhibit greater hover efficiency than the baseline propeller. This trend can be attributed to the largest chord length closer to or at 50% to 90% of the spanwise, which is known as the lift booster area, and means the bioinspired planforms are beneficial in terms of aerodynamic efficiency. Compared to other bioinspired propellers, the Neuroptera propeller produced more thrust and showed higher hover efficiency.

3.2. Acoustic Signature Results

The aeroacoustic signature is characterized by an overall A-weighted sound pressure level (OASPL) at different frequencies and is calculated by Equations (6) and (7). Where SPL_A is A-weighted sound pressure level, $p_A(t)$ is the instantaneous sound pressure measured using the standard frequency weighting A, and p_{ref} is the reference pressure and equal to $2 \times 10^{-5}\ Pa$.

$$OASPL = 10log \sum_{i=1}^{n} 10^{\frac{SPL_A}{10}} \tag{6}$$

$$SPL_A = 20 \log \left(\frac{p_A(t)}{p_{ref}} \right) \tag{7}$$

As shown in Fig. 7, mechanical noise (no propeller) has little influence at low frequencies (2500 Hz) but grows significantly above that frequency. Clearly, motor noise plays a key role in the system's stress noise at low frequencies. Also, Fig. 7 shows that the bioinspired propellers can decrease harmonic and broadband noise more effectively than the baseline propeller at hover flight with 3N thrust. Harmonic noise is associated with blade passing frequency and consists of loading and thickness noise. When the Mach number is less than one, the loading noise takes precedence over the harmonic noise. However, it can decrease broadband noise more effectively than the baseline propeller at higher frequencies, due to the effect of the bioinspired planforms on the velocity gradient and pushing the wake vortices further from the trailing edge. This phenomenon reduces turbulent-boundary layer trailing edge noise and vortex shedding noise at the trailing

edge and decreases inter-mode interference involving modes from the propeller apparent at higher frequencies. To better illustrate the differences in the graphs, the original graphs are shown in transparent and the ninth degree polynomial is shown in bold. This analysis helps to understand the noise characteristics of the bioinspired planforms.

Figure 8 shows the OASPL directivity plot at hover flight with 3N thrust. As we move up and down from microphone number five, the noise increases, which shows the loading, broadband, and blade-vortex interaction noise have overcome the thickness noise. The microphones on the roll plane show a distinct level of noise increasing and more noise emitting at the top of the roll plane. There is a slight variation in rotor plane microphone noises. As long as there is no interference from another rotor, the noise is virtually constant throughout the rotor plane.

Figure 9 indicates changing OASPL values of microphone number five versus RPM and thrust to evaluate the overall noise reduction. At microphone number five, when the rotational speed increase from 3000 RPM to 8000 RPM, the OASPL of the baseline propeller increase from 42.3 dBA to 64.4 dBA, the Blattodea propeller increase from 40.5 dBA to 63.4 dBA, the Hemiptera propeller increase from 40.5 dBA to 62.9 dBA, the Hymenoptera propeller increase from 41.8 dBA to 64.5 dBA, the Maple Seed propeller increase from 40.2 dBA to 62.4 dBA, the Neuroptera propeller increase from 40.6 dBA to 64.3 dBA, and the Odonata propeller increase from 40.9 dBA to 62.1 dBA. Due to the difference in the generated thrust at the same RPM, the sound produced by the bioinspired propellers is lower than the baseline propeller in all thrust ranges.

The OASPL at hover fight with 3N thrust for Neuroptera propeller is 52.5 dBA, for Odonata propeller is 53.5 dBA, for Hymenoptera propeller is 54.2 dBA, for Hemiptera and Maple Seed propellers are 55.4 dBA, for Blattodea propeller is 56.9 dBA, and for baseline propeller is 60.4 dBA. Therefore, the results indicate that the Neuroptera propeller generates 7.9 dBA, the Odonata propeller generates 6.9 dBA, the Hymenoptera propeller generates 6.2 dBA, the Hemiptera and Maple Seed propeller generates 5 dBA, and the Blattodea propeller generates 3.5 dBA less noise than the baseline propeller at microphone number five and hover condition with 3N thrust.

3.3. Aeroacoustic Results Compared to The T9545 Propeller

Figure 10 presents the comparative aerodynamic and aeroacoustic performance results. When the rotational speed increase from 3000 RPM to 8000 RPM, the time-averaged thrust of the T9545 propeller increases from 0.79N to 5.63N, and the power loading of the T9545 propeller increases from 0.11 N/W to 0.28 N/W. Therefore, the power loading of the T9545 propeller in all RPM and thrust ranges is higher than the baseline and lower than the Neuroptera, Hymenoptera, and Odonata propellers.

At hover flight with 3N thrust, the rotational speed of the T9545 propeller is 5777 RPM, which shows this propeller is 21.4Hz slower than the baseline propeller, and 15.3Hz faster than the Neuroptera propeller, 9.6Hz faster than the Hymenoptera propeller, and 5.3Hz faster than the Odonata propeller at the same thrust.

Further, the required time-averaged power of the T9545 propeller at hover flight with 3N thrust is 14.5W. The results indicate that the T9545 propeller consumes 2.3W more power than the Neuroptera propeller, 1.4W more power than the Hymenoptera propeller, 0.8W more power than the Odonata propeller, and 0.3W less power than the Blattodea and Hemiptera propeller, 0.8W less power than the Maple Seed propeller, 3.2W less power than the baseline propeller at hover flight. With a maximum power decrease of 18% at hover flight, the T9545 propeller performs better than the baseline propeller. This propeller performs worse than Neuroptera, Hymenoptera, and Odonata propellers with maximum power increase of 13%, 8.2%, and 4.6% at hover flight, respectively. In conclusion, at hover flight with 3N thrust, the power loading of this propeller is 0.21 N/W.

Furthermore, the figure of merit of the T9545 propeller at hover flight with 3N thrust is 3.05. The figure of merit of the T9545 propeller at this thrust is about 9.3% higher than the baseline propeller. The figure of merit of the T9545 propeller is lower than the other propellers.

The results demonstrate that the T9545 propeller produces more thrust than the baseline, Blattodea, Maple Seed, and Hemiptera propellers and less thrust than the Hymenoptera, Neuroptera, and Odonata propellers for the same power supply. Also, T9545 propeller generates less drag than the baseline, Blattodea, Hemiptera, and Maple Seed propellers and more drag than the Hymenoptera, Neuroptera, and Odonata propellers at hover flight with 3N thrust.

The OASPL of the T9545 propeller at microphone number five increases from 38.3 dBA to 62.5 dBA when the rotational speed increase from 3000 RPM to 8000 RPM. Also, the OASPL at hover fight with 3N thrust for this propeller is 51.5 dBA. Therefore, the results indicate that the T9545 propeller generates noise 1.0 dBA less than the Neuroptera propeller, 2.0 dBA less than the Odonata propeller, 2.7 dBA less than the Hymenoptera propeller, 3.8 dBA less than the Maple Seed propeller, 3.9 dBA less than the Hymenoptera propeller, 5.4 dBA less than the Blattodea propeller, and 8.9 dBA less than the baseline propeller at microphone number five and hover condition with 3N thrust.

Aeroacoustic results reveal that bioinspired propellers perform better than baseline and T9545 propellers. It should be noted that the designed propellers have lower manufacturing quality than the T9545 propeller. It is expected that by increasing the manufacturing quality, the results of all propellers will improve, and the baseline propeller shows results that are closer to those of the T9545 propeller.

4. Conclusions

An experimental investigated the impacts of operation conditions and varied geometric parameters on six small propellers' aerodynamic and aeroacoustic performance with a unique planform shape inspired by five insects and one plant, such as Blattodea, Hemiptera, Hymenoptera, Neuroptera, Odonata, and Maple Seed. Each propeller was operated at eleven rotational speeds ranging from 3000 to 8000 RPM with no freestream velocity for simulating hover conditions. Finally, using force and sound, a comparative experimental investigation into the aerodynamics and aeroacoustics characteristics of the baseline and bioinspired propellers was undertaken in an anechoic chamber. Compared to the baseline propeller, the results demonstrate that all bioinspired propellers produce more thrust for the same power supply, reduce harmonic and broadband noise, and provide a better noise level. This noise reduction can be ascribed to the decreasing bioinspired propeller force variation. Also, their rotational speed is lower and their figure of merit is higher than the baseline propeller at hover flight with 3N thrust. They all outperform the baseline propeller in terms of hover efficiency at all thrust values considered. Besides, the Neuroptera propeller is more efficient than other propellers, decreasing 5.5W of power and reducing 7.9 dBA at hover flight with 3N thrust and 1.5 meters distance, compared to the baseline propeller.

Future investigations will focus on some improvements. XFoil should be utilized to guarantee that the best airfoil is chosen for each blade segment. Because noise generation is affected by blade quality vibrations, a high-resolution (25μm) 3D printed using a rigid material such as ABS plastic might offer accurate manufacturing precision. To increase structural stiffness, the airfoil section from $r/R = 0.2$ should be smoothly integrated into the hub. To ensure reliable printing output, the trailing edge airfoil utilized along the propeller span (E63) should be thickened to 0.8 mm. The propeller should be connected from the top to a profiled aluminum testing rig for the least amount of interference. To decrease motor and test stand vibrations, a neoprene dampening material should be put directly beneath the load cell. The sampling rate may be increased to 80 kHz. The recording time may be increased by up to 20 seconds, and the data from the first 10 seconds could be utilized to compute acoustic spectra. It is necessary to investigate the effects of recirculation within the anechoic chamber. To get a frequency resolution of around 5 Hz, the number of FFT samples might be increased.

This study did not assess the influence of the existence of adjacent propellers and forward flight, which makes them a great target for future investigations. Furthermore, Smoke visualization, hotwire mapping, and PIV might be used to describe the downwash flow of a propeller, among other methods.

Declaration of Conflicting Interests

The authors declare that there is no conflict of interest.

References

[1] Science for Environmental Policy, "FUTURE BRIEF: Noise Abatement Approaches," *EU Publ.*, no. 17, pp. 3–25, Apr. 2017, doi: 10.2779/016648.

[2] R. S. McKay and M. J. Kingan, "Multi-rotor unmanned aerial system noise: Quantifying the motor's contribution," in *24th Acoustical Society of New Zealand Conference*, 2018, no. 1.

[3] W. N. Alexander, J. Whelchel, N. Intaratep, and A. Trani, "Predicting community noise of sUAS," in *25th AIAA/CEAS Aeroacoustics Conference, 2019*, 2019, doi: 10.2514/6.2019-2686.

[4] N. Intaratep, W. Nathan Alexander, W. J. Deveport, S. M. Grace, and A. Dropkin, "Experimental study of quadcopter acoustics and performance at static thrust conditions," in *22nd AIAA/CEAS Aeroacoustics Conference, 2016*, 2016, doi: 10.2514/6.2016-2873.

[5] N. S. Zawodny, D. D. Boyd, and C. L. Burley, "Acoustic characterization and prediction of representative, small-scale rotary-wing unmanned aircraft system components," in *Annual Forum Proceedings - AHS International*, 2016, vol. 1–2016, pp. 34–48.

[6] S. E. Wright, "The acoustic spectrum of axial flow machines," *J. Sound Vib.*, vol. 45, no. 2, pp. 165–223, 1976, doi: 10.1016/0022-460X(76)90596-4.

[7] N. S. Zawodny and D. D. Boyd, "Investigation of rotor–airframe interaction noise associated with small-scale rotary-wing unmanned aircraft systems," *J. Am. Helicopter Soc.*, vol. 65, no. 1, 2020, doi: 10.4050/JAHS.65.012007.

[8] J. Whelchel, W. N. Alexander, and N. Intaratep, "Propeller noise in confined anechoic and open environments," in *AIAA Scitech 2020 Forum*, 2020, vol. 1 PartF, doi: 10.2514/6.2020-1252.

[9] J. Brandt and M. Selig, "Propeller Performance Data at Low Reynolds Numbers," 2011, doi: 10.2514/6.2011-1255.

[10] C. F. Wisniewski, A. R. Byerley, K. W. Van Treuren, and A. Hays, "Experimentally testing commercial and custom designed Quadcopter propeller static performance and noise generation," in *23rd AIAA/CEAS Aeroacoustics Conference, 2017*, 2017, doi: 10.2514/6.2017-3711.

[11] R. S. McKay and M. J. Kingan, "Multirotor unmanned aerial system propeller noise caused by unsteady blade motion," in *25th AIAA/CEAS Aeroacoustics Conference, 2019*, 2019, doi: 10.2514/6.2019-2499.

[12] N. S. Zawodny and H. H. Haskin, "Small propeller and rotor testing capabilities of the NASA langley low speed aeroacoustic wind tunnel," in *23rd AIAA/CEAS Aeroacoustics Conference, 2017*, 2017, doi: 10.2514/6.2017-3709.

[13] G. Andria *et al.*, "Design and performance evaluation of drone propellers," in *5th IEEE International Workshop on Metrology for AeroSpace, MetroAeroSpace 2018 - Proceedings*, 2018, pp. 407–412, doi: 10.1109/MetroAeroSpace.2018.8453604.

[14] G. Sinibaldi and L. Marino, "Experimental analysis on the noise of propellers for

small UAV," *Appl. Acoust.*, vol. 74, no. 1, pp. 79–88, 2013, doi: 10.1016/j.apacoust.2012.06.011.

[15] Y. Yang, Y. Wang, Y. Liu, H. Hu, and Z. Li, "Noise reduction and aerodynamics of isolated multi-copter rotors with serrated trailing edges during forward flight," *J. Sound Vib.*, vol. 489, 2020, doi: 10.1016/j.jsv.2020.115688.

[16] A. Cambray, E. Pang, S. A. Showkat Ali, D. Rezgui, and M. Azarpeyvand, "Investigation towards a better understanding of noise generation from UAV propellers," in *2018 AIAA/CEAS Aeroacoustics Conference*, 2018, doi: 10.2514/6.2018-3450.

[17] Z. Ning, R. Wlezien, and H. Hu, "An experimental study on small UAV propellers with serrated trailing edges," in *47th AIAA Fluid Dynamics Conference, 2017*, 2017, doi: 10.2514/6.2017-3813.

[18] J. Xiong, N. Nguyen, and N. B. Cramer, "Acoustic optimization for anti-phase asymmetric rotor," in *AIAA Scitech 2020 Forum*, 2020, vol. 1 PartF, doi: 10.2514/6.2020-1496.

[19] Y. Yang *et al.*, "Experimental study on noise reduction of a wavy multi-copter rotor," *Appl. Acoust.*, vol. 165, 2020, doi: 10.1016/j.apacoust.2020.107311.

[20] C. Hintz, P. Khanbolouki, A. M. Perez, M. Tehrani, and S. V. Poroseva, "Experimental study of the effects of bio-inspired blades and 3D printing on the performance of a small propeller," in *2018 Applied Aerodynamics Conference*, 2018, doi: 10.2514/6.2018-3645.

[21] Z. Ning and H. Hu, "An experimental study on the aerodynamic and aeroacoustic performances of a bio-inspired UAV propeller," in *35th AIAA Applied Aerodynamics Conference, 2017*, 2017, doi: 10.2514/6.2017-3747.

[22] Z. J. Wang, "Two dimensional mechanism for insect hovering," *Phys. Rev. Lett.*, vol. 85, no. 10, pp. 2216–2219, 2000, doi: 10.1103/PhysRevLett.85.2216.

[23] J. Young, S. M. Walker, R. J. Bomphrey, G. K. Taylor, and A. L. R. Thomas, "Details of insect wing design and deformation enhance aerodynamic function and flight efficiency," *Science (80-.).*, vol. 325, no. 5947, pp. 1549–1552, 2009, doi: 10.1126/science.1175928.

[24] M. J. Ringuette, M. Milano, and M. Gharib, "Role of the tip vortex in the force generation of low-aspect-ratio normal flat plates," *J. Fluid Mech.*, vol. 581, pp. 453–468, 2007, doi: 10.1017/S0022112007005976.

Figure Captions List

Table Caption List

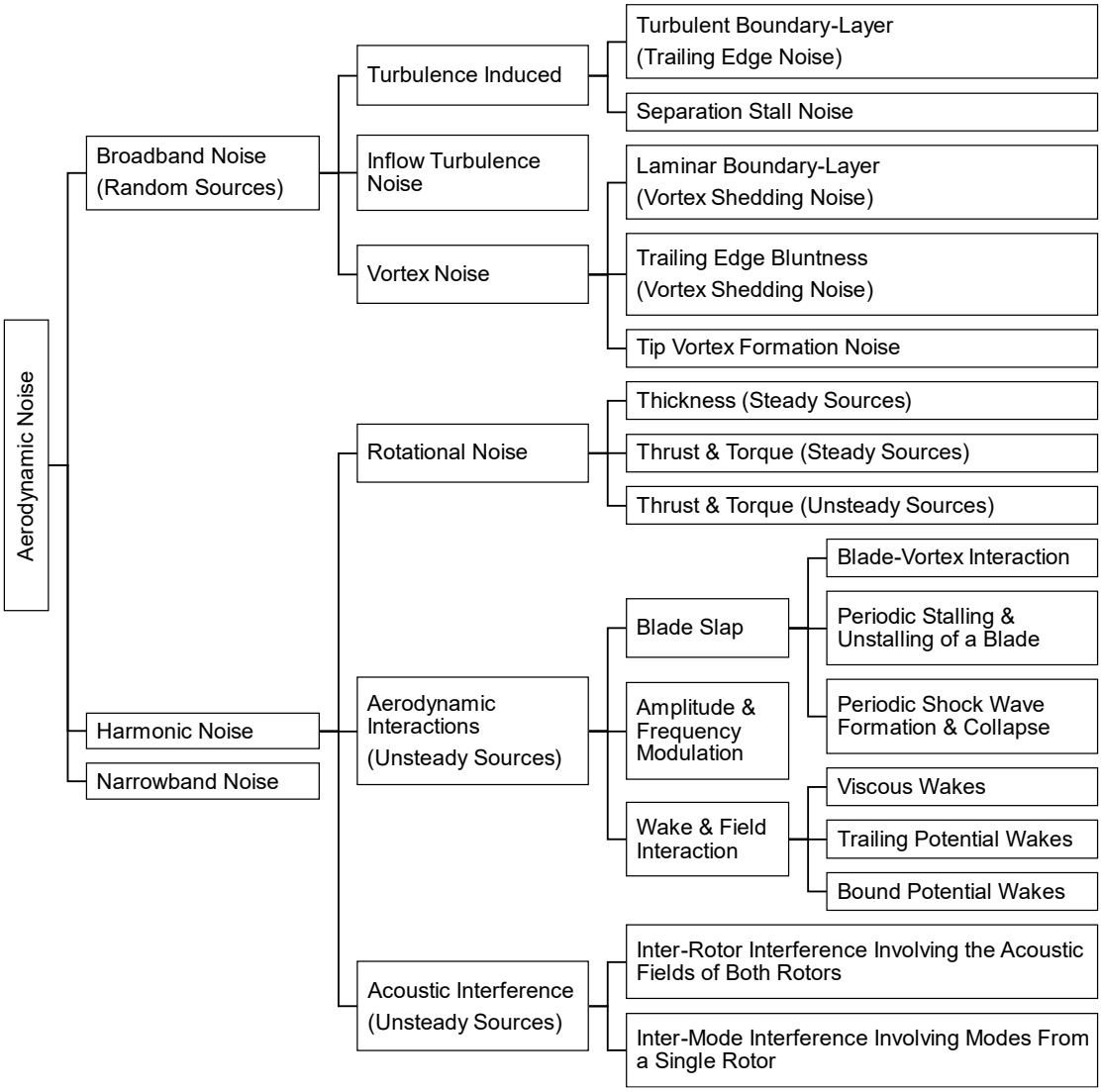

Fig. 1 Aerodynamic noise sources

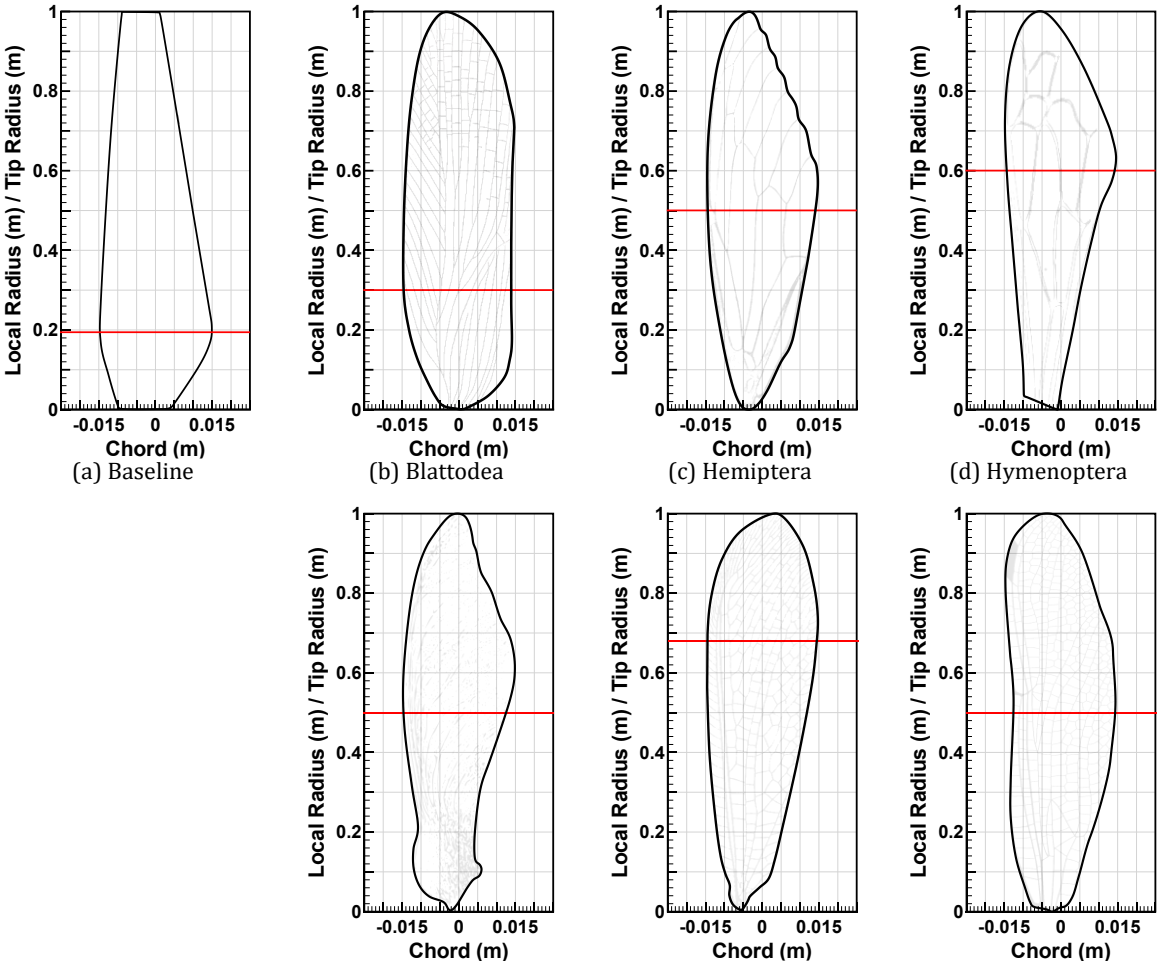

(a) Baseline (b) Blattodea (c) Hemiptera (d) Hymenoptera

(e) Maple Seed (f) Neuroptera (g) Odonata

Fig. 2 Baseline and bioinspired wing planforms and their maximum chord location

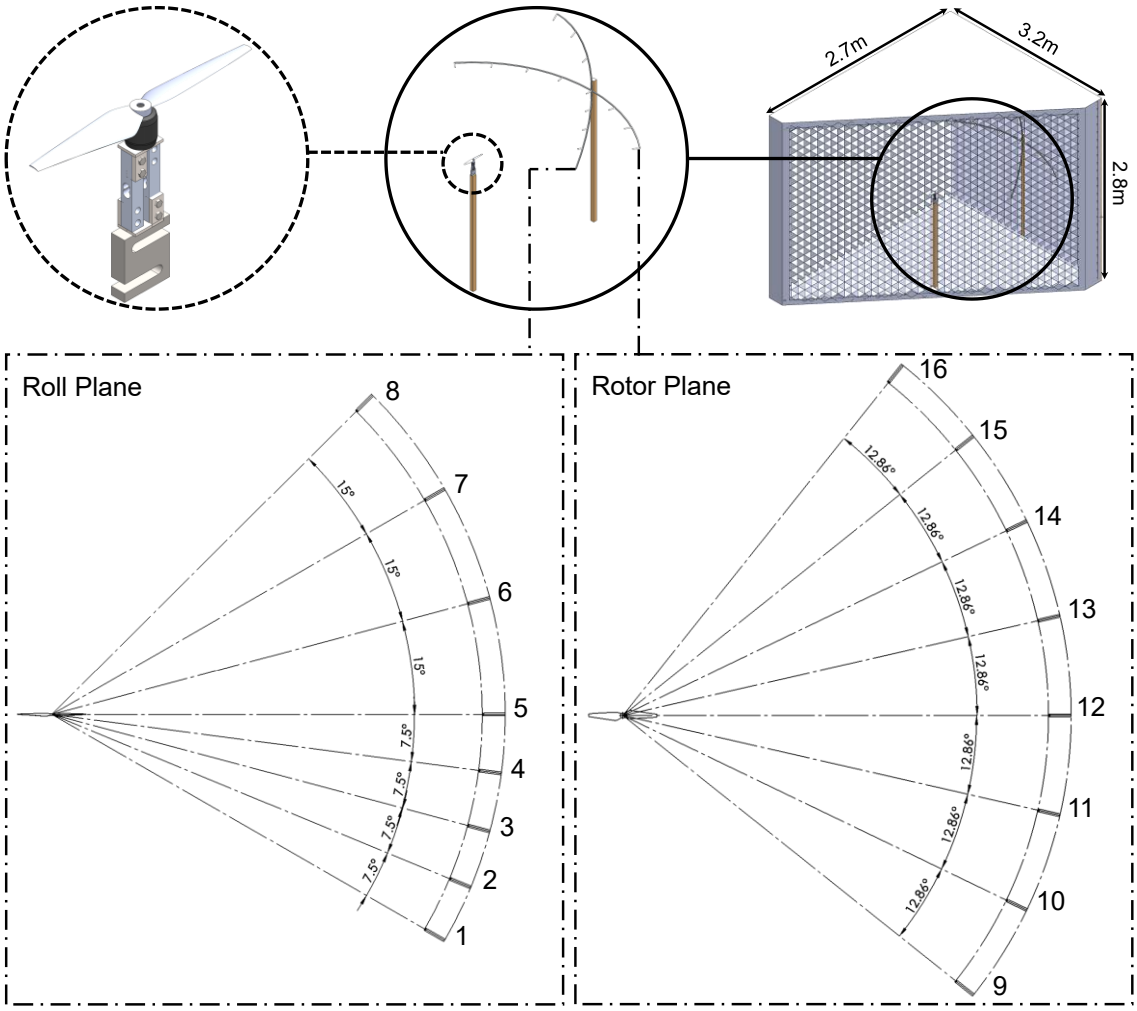

Fig. 3 Schematic of the facilities and microphone array

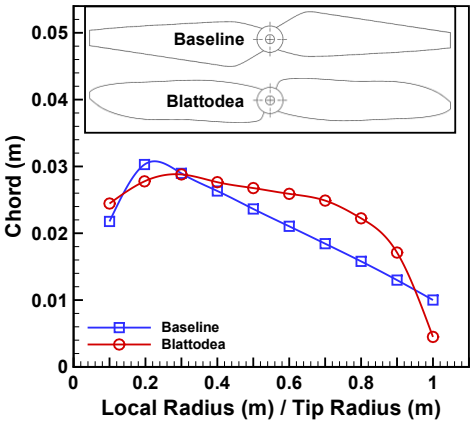

(a) Baseline and Blattodea

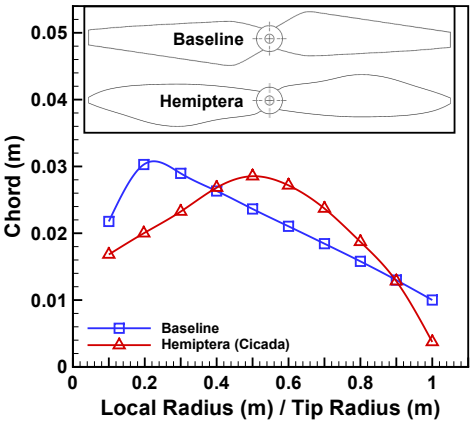

(b) Baseline and Hemiptera

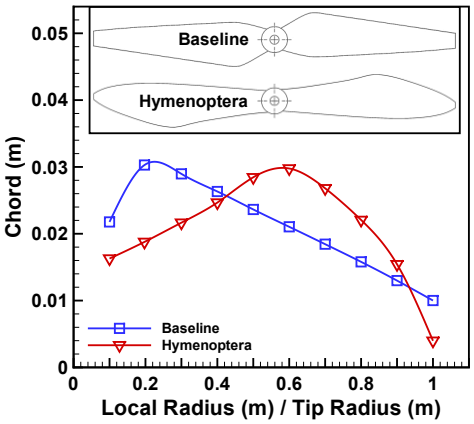

(c) Baseline and Hymenoptera

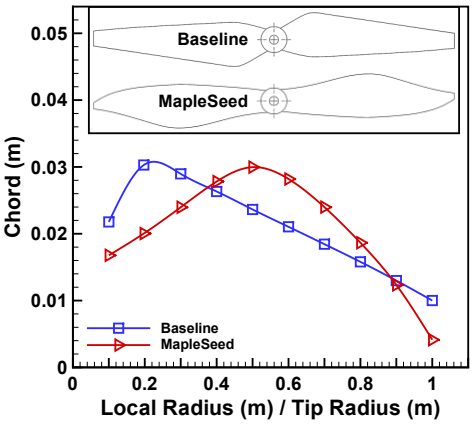

(d) Baseline and MapleSeed

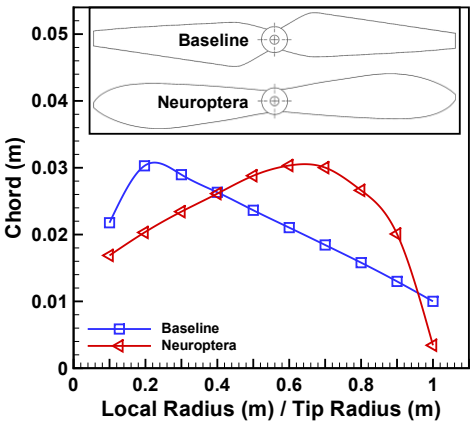

(e) Baseline and Neuroptera

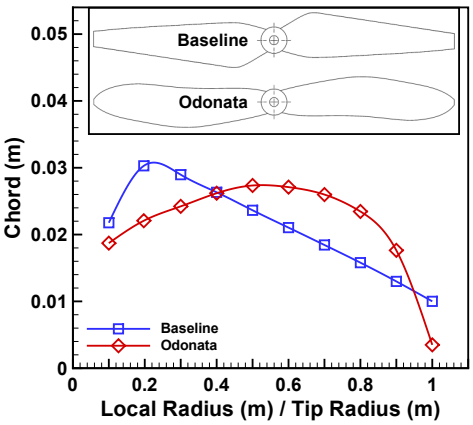

(f) Baseline and Odonata

Fig. 4 Schematic and chord distribution of propellers compared to the baseline propeller

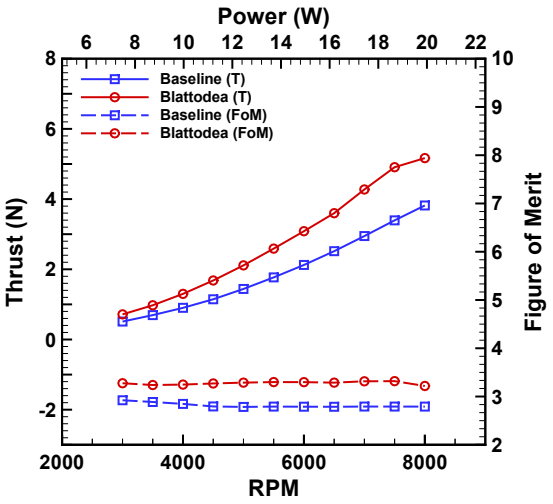

(a) Baseline and Blattodea

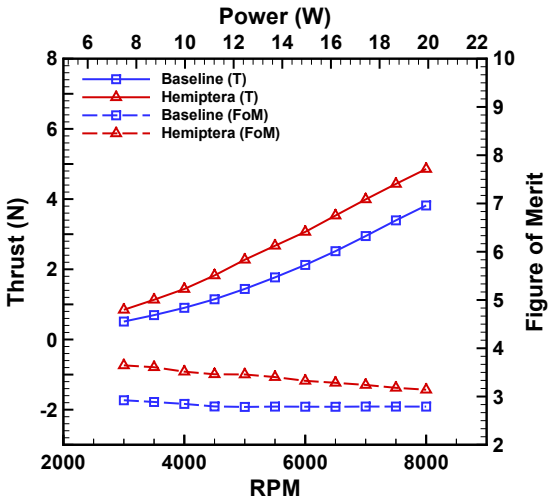

(b) Baseline and Hemiptera

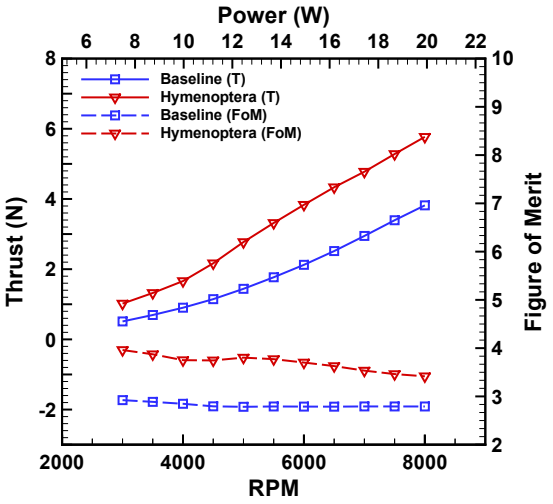

(c) Baseline and Hymenoptera

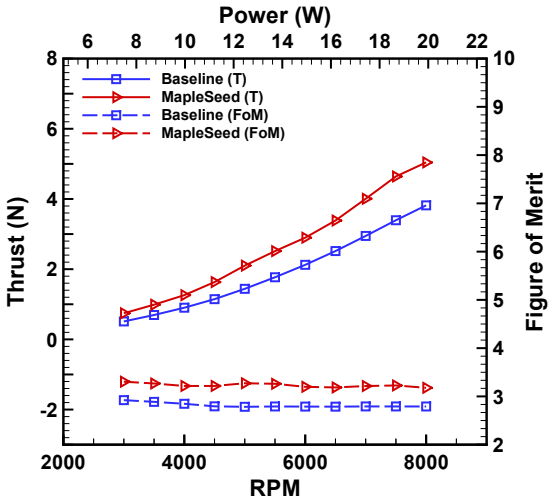

(d) Baseline and MapleSeed

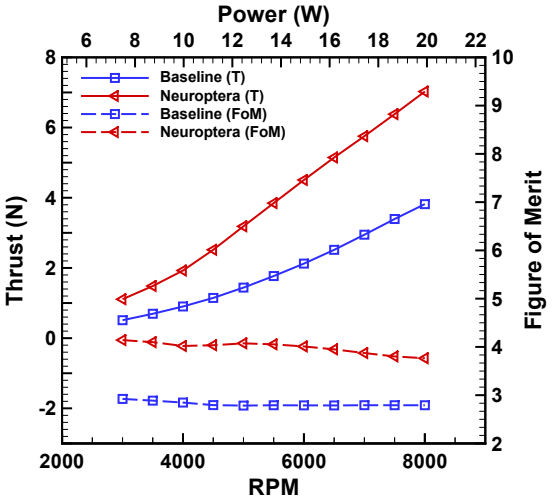

(e) Baseline and Neuroptera

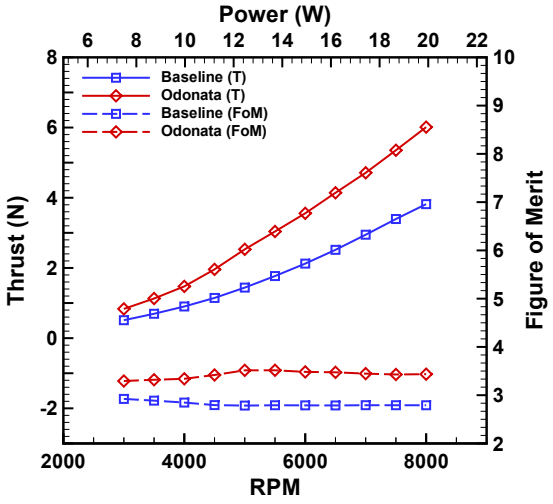

(f) Baseline and Odonata

Fig. 5 Aerodynamic performance results compared to the baseline propeller

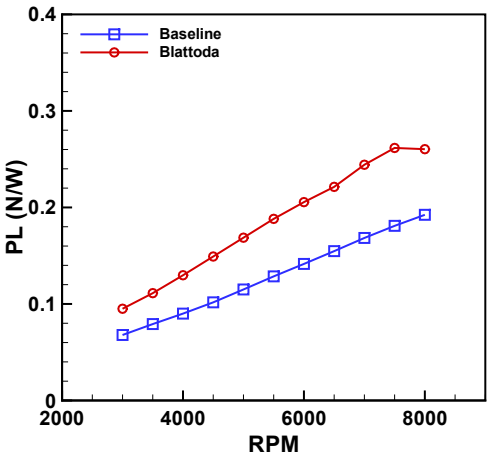

(a) Baseline and Blattodea

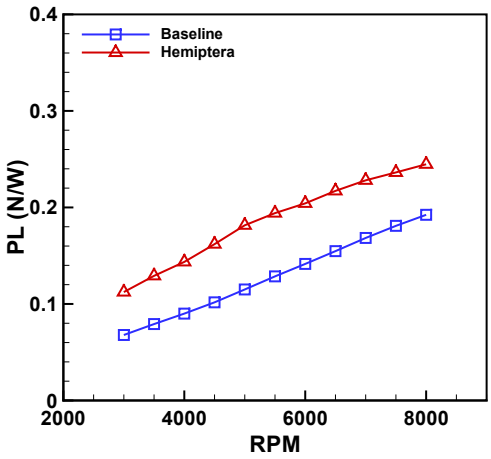

(b) Baseline and Hemiptera

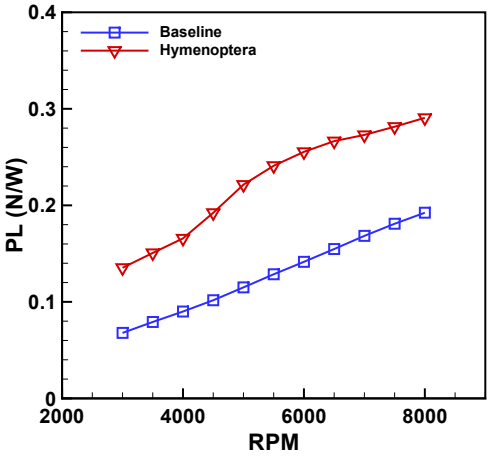

(c) Baseline and Hymenoptera

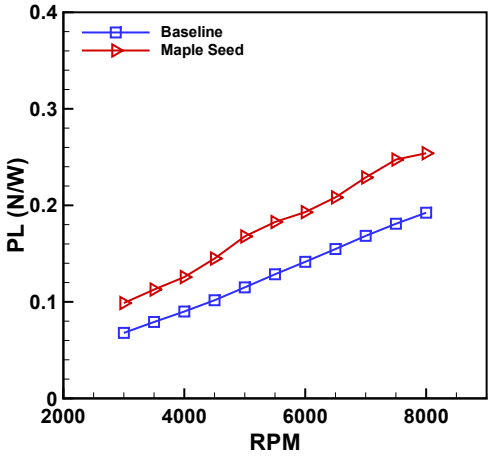

(d) Baseline and MapleSeed

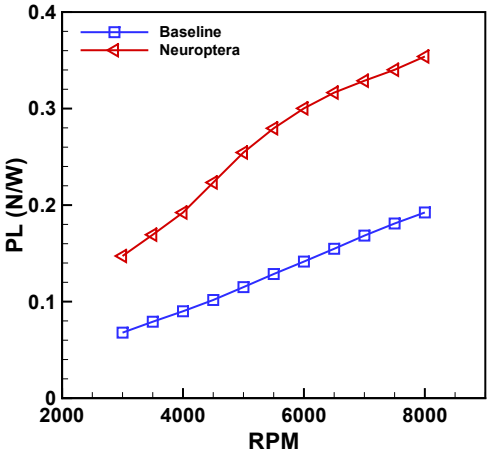

(e) Baseline and Neuroptera

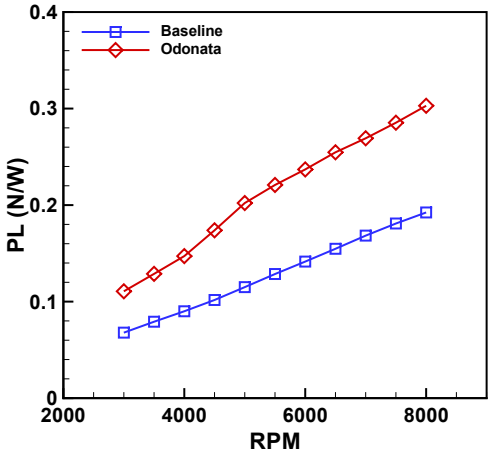

(f) Baseline and Odonata

Fig. 6 Power loading results compared to the baseline propeller

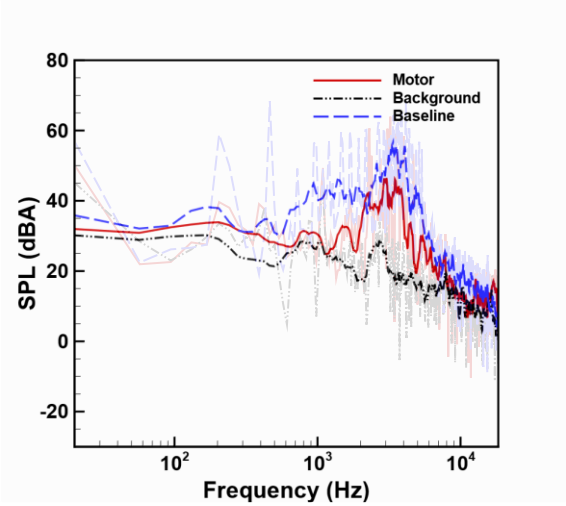

(a) Baseline, Background, and Motor

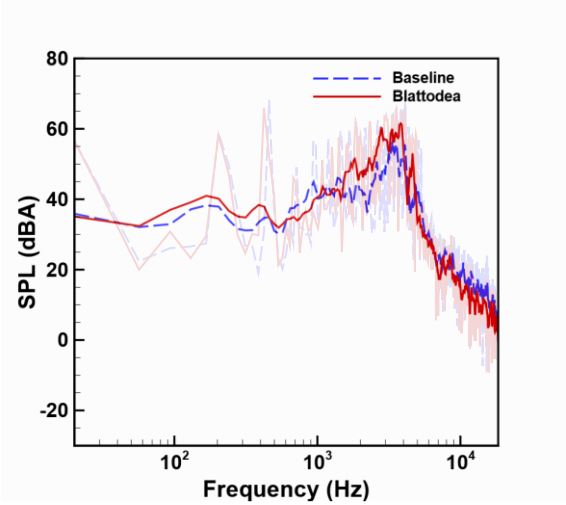

(b) Baseline and Blattodea

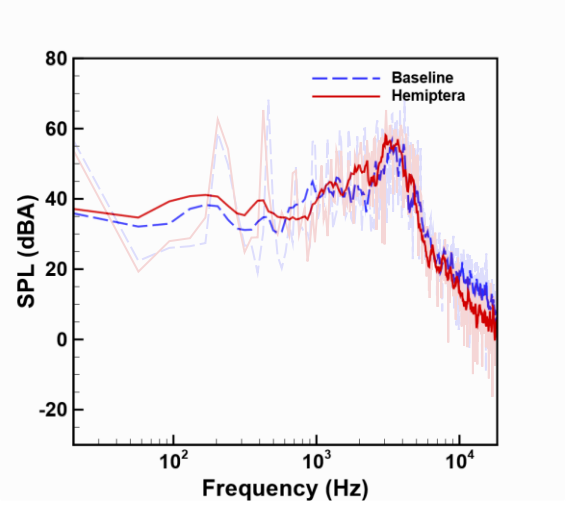

(c) Baseline and Hemiptera

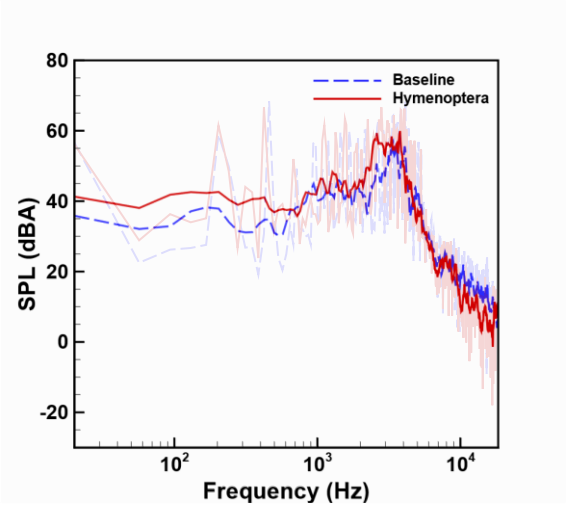

(d) Baseline and Hymenoptera

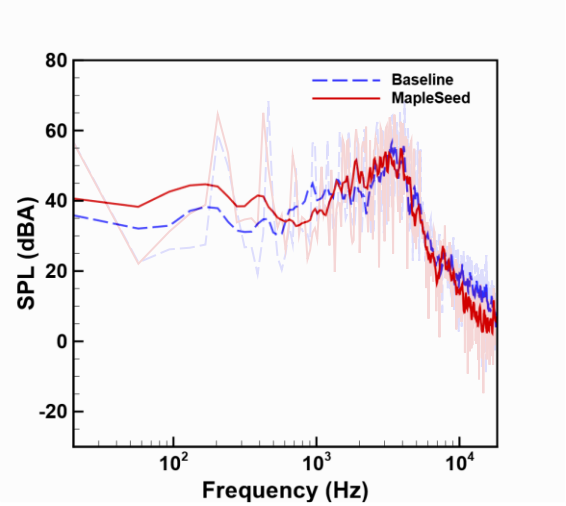

(e) Baseline and Maple Seed

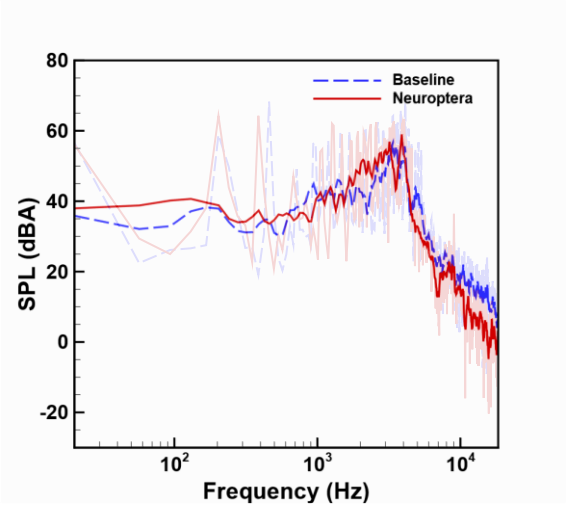

(f) Baseline and Neuroptera

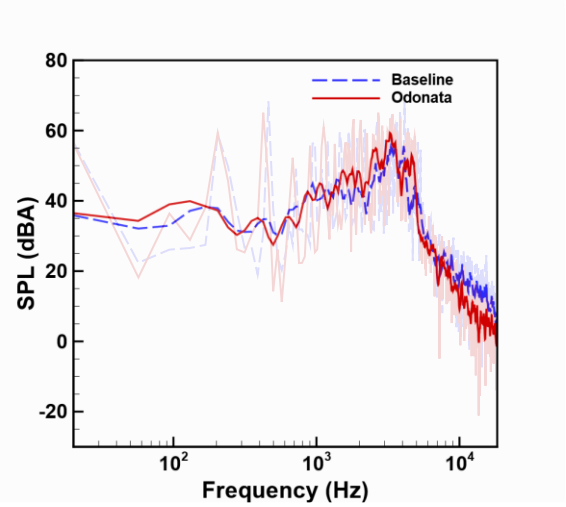

(g) Baseline and Odonata

Fig. 7 Acoustic signature results compared to the baseline propeller at hover flight with 3N thrust (To better illustrate the differences in the graphs, the original graphs are shown in transparent and the ninth degree polynomial is shown in bold.)

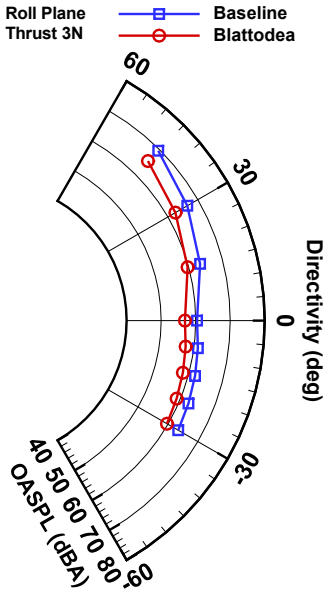

(a) Baseline and Blattodea roll plane directivity comparison

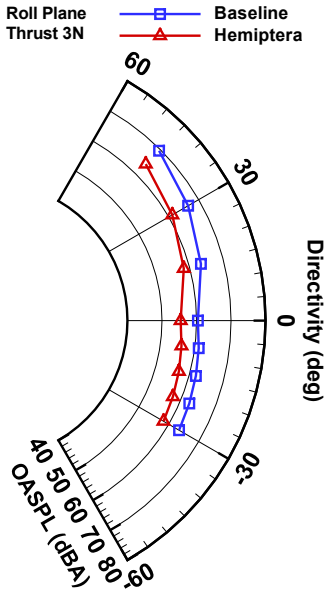

(b) Baseline and Hemiptera roll plane directivity comparison

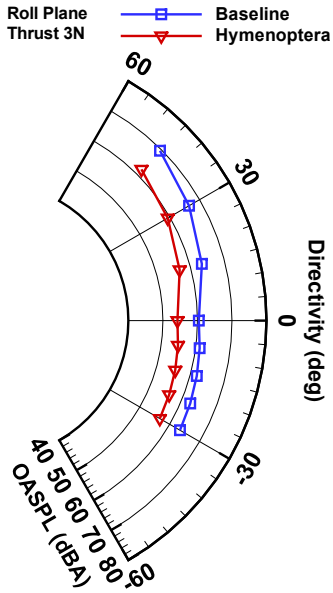

(c) Baseline and Hymenoptera roll plane directivity comparison

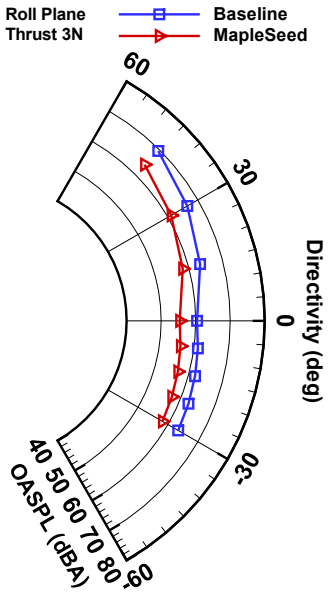

(d) Baseline and Maple Seed roll plane directivity comparison

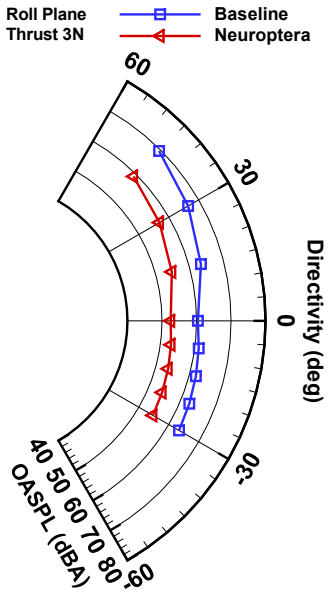

(e) Baseline and Neuroptera roll plane directivity comparison

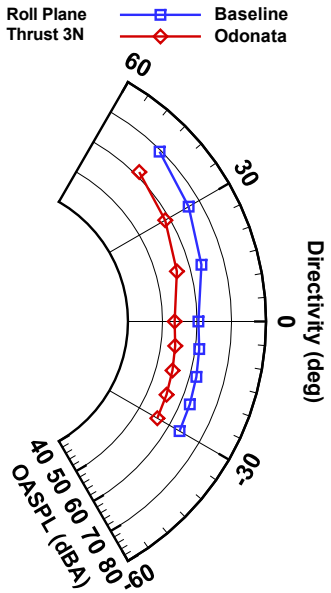

(f) Baseline and Odonata roll plane directivity comparison

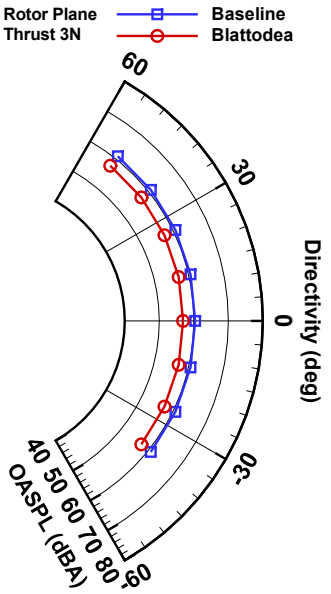

(g) Baseline and Blattodea rotor plane directivity comparison

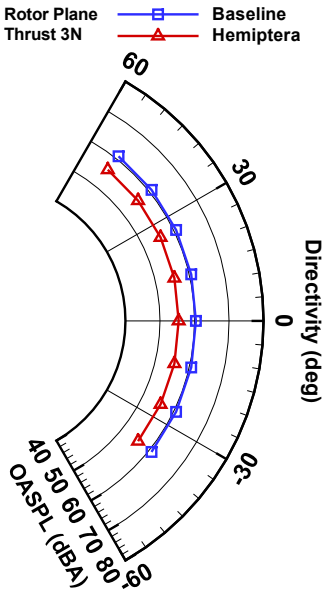

(h) Baseline and Hemiptera rotor plane directivity comparison

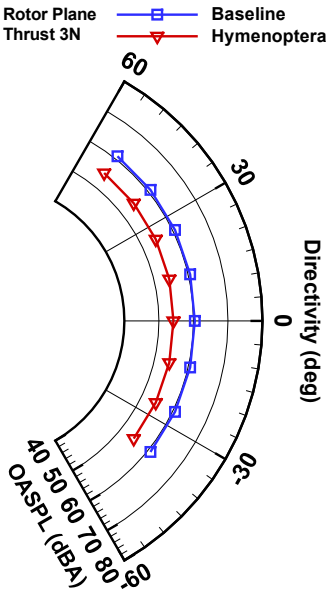

(i) Baseline and Hymenoptera rotor plane directivity comparison

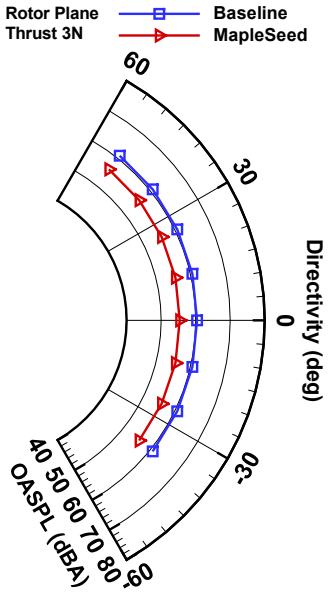

(j) Baseline and Maple Seed rotor plane directivity comparison

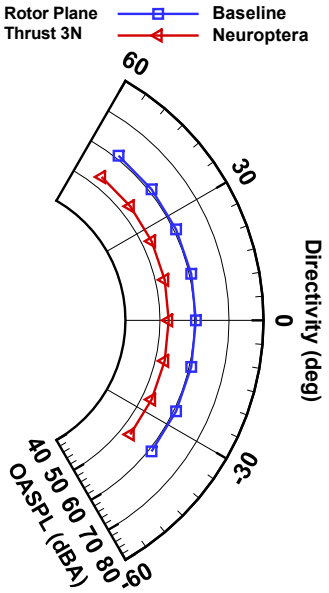

(k) Baseline and Neuroptera rotor plane directivity comparison

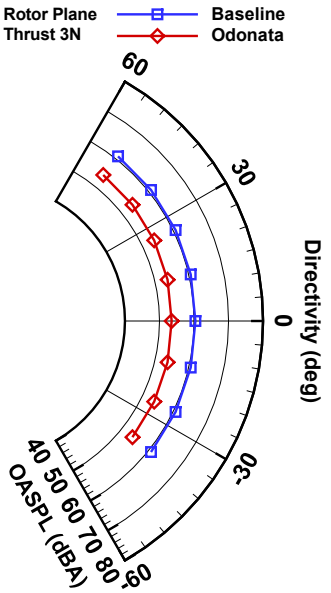

(l) Baseline and Odonata rotor plane directivity comparison

Fig. 8 Bioinspired propellers noise directivity at hover flight with 3N thrust compared to the baseline propeller

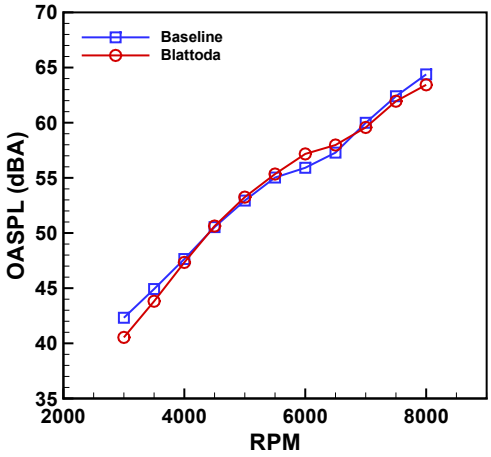

(a) OASPL of baseline and Blattodea propellers comparison in RPM

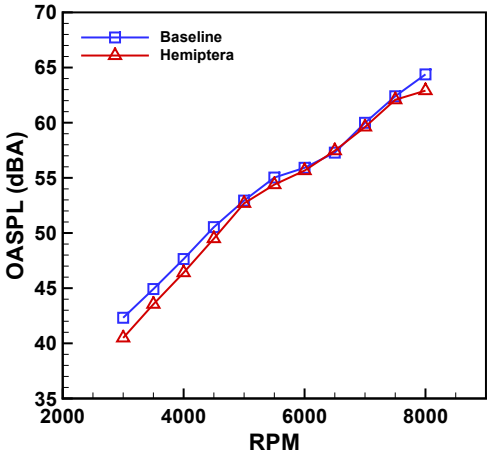

(b) OASPL of baseline and Hemiptera propellers comparison in RPM

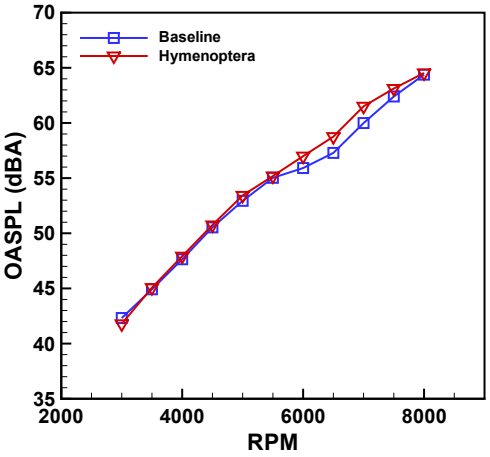

(c) OASPL of baseline and Hymenoptera propellers comparison in RPM

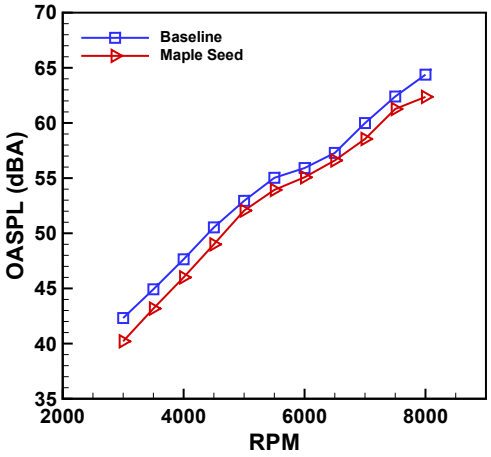

(d) OASPL of baseline and Maple Seed propellers comparison in RPM

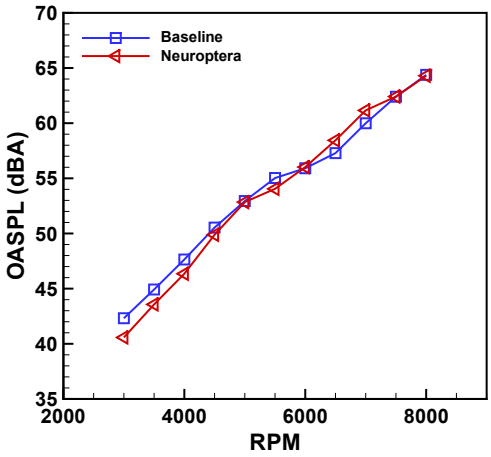

(e) OASPL of baseline and Neuroptera propellers comparison in RPM

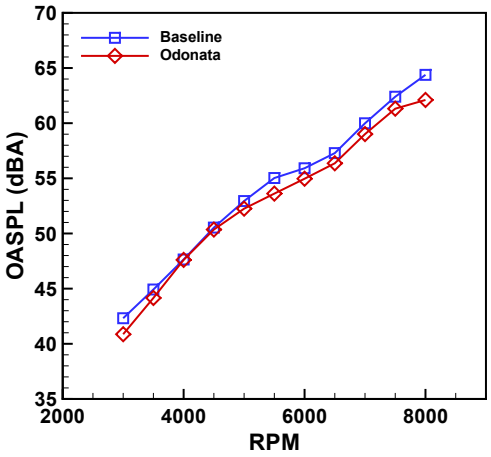

(f) OASPL of baseline and Odonata propellers comparison in RPM

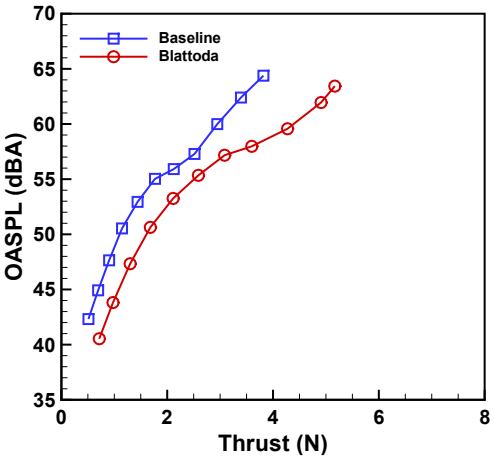

(g) OASPL of baseline and Blattodea propellers comparison in thrust

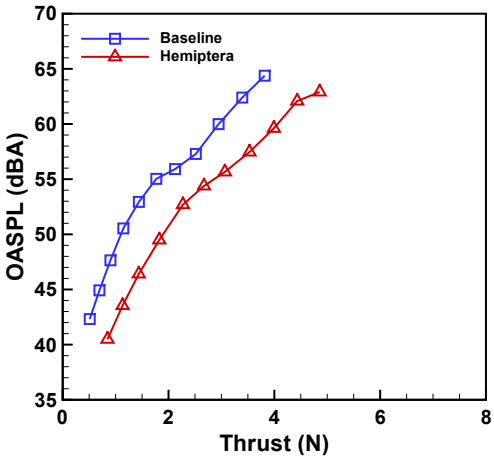

(h) OASPL of baseline and Hemiptera propellers comparison in thrust

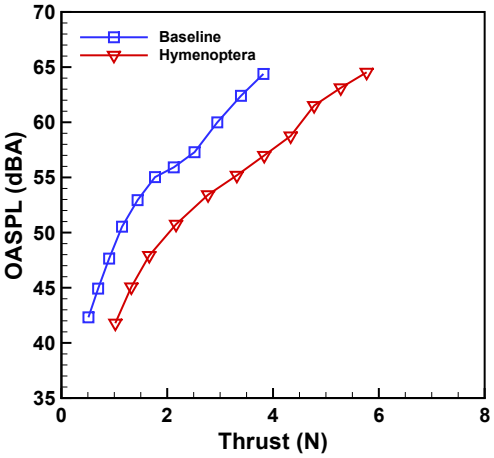

(i) OASPL of baseline and Hymenoptera propellers comparison in thrust

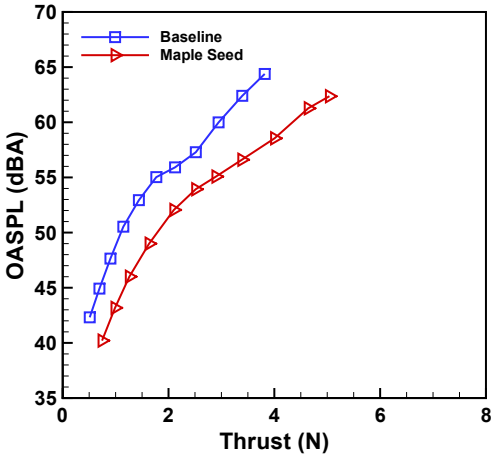

(j) OASPL of baseline and Maple Seed propellers comparison in thrust

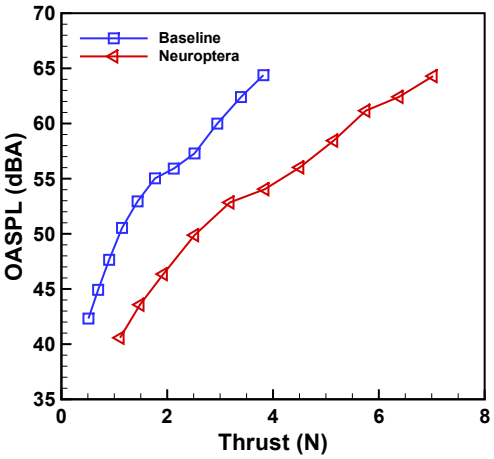

(k) OASPL of baseline and Neuroptera propellers comparison in thrust

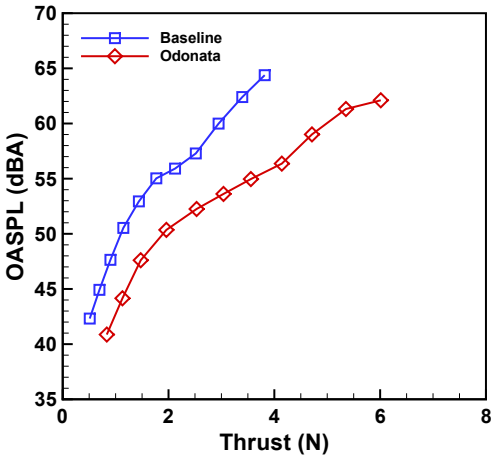

(l) OASPL of baseline and Odonata propellers comparison in thrust

Fig. 9 Aeroacoustic performance results compared to the baseline propeller at microphone number five

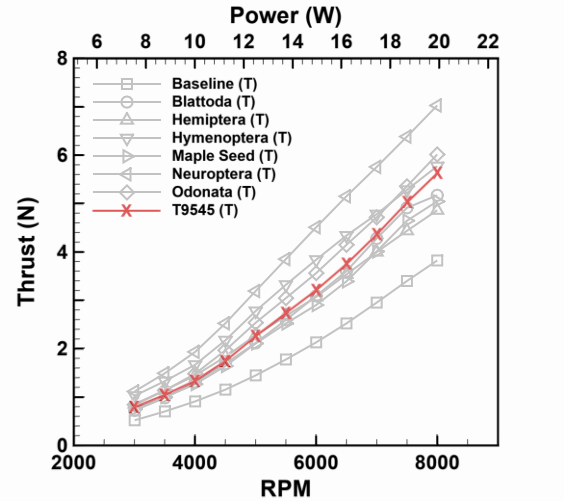

(a) Thrust of bioinspired propellers compared to the T9545 propeller

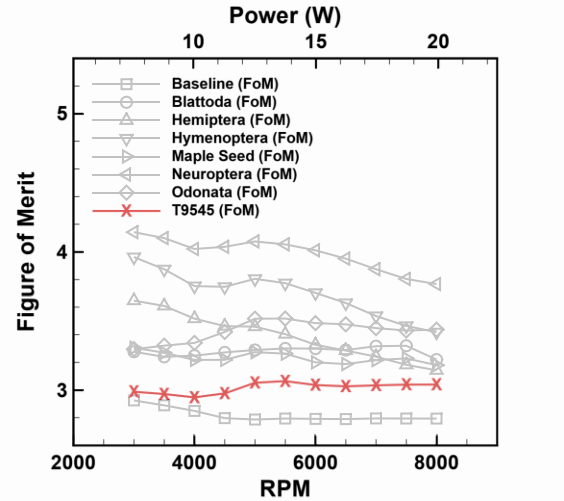

(b) Figure of merit of bioinspired propellers compared to the T9545 propeller

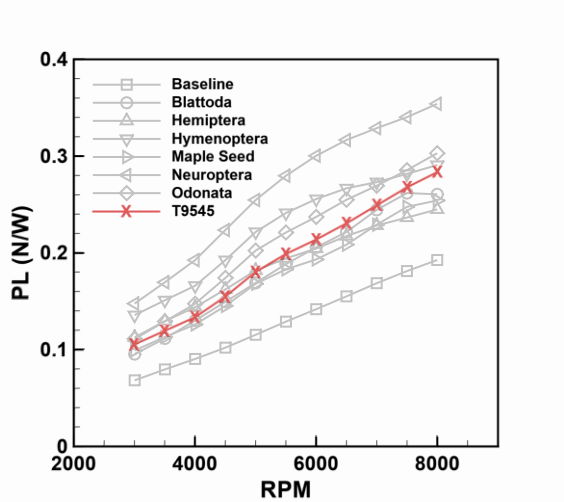

(c) Power loading of bioinspired and T9545 propellers comparison in RPM

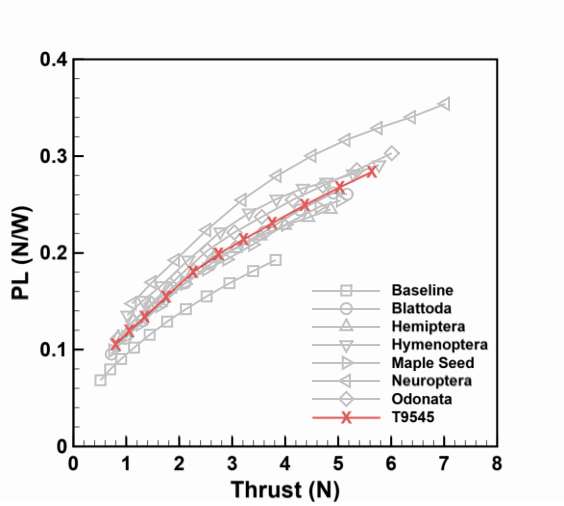

(d) Power loading of bioinspired and T9545 propellers comparison in Thrust

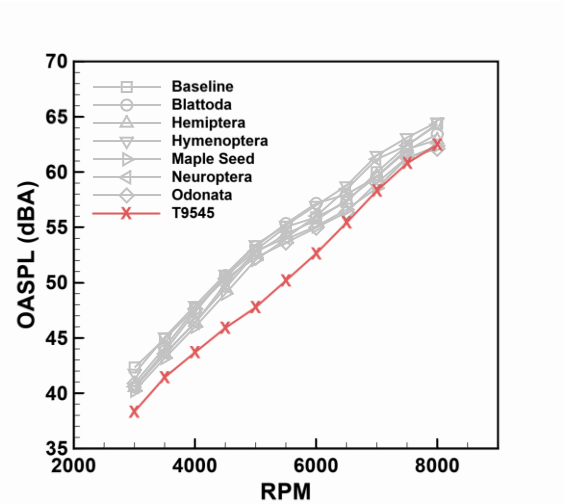

(e) OASPL of bioinspired and T9545 propellers comparison in RPM

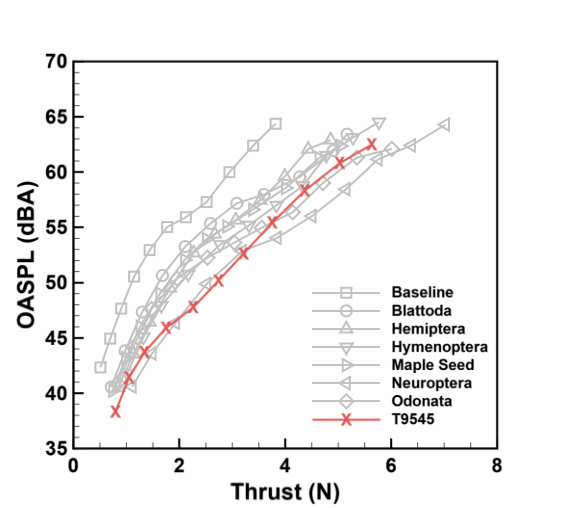

(f) OASPL of bioinspired and T9545 propellers comparison in Thrust

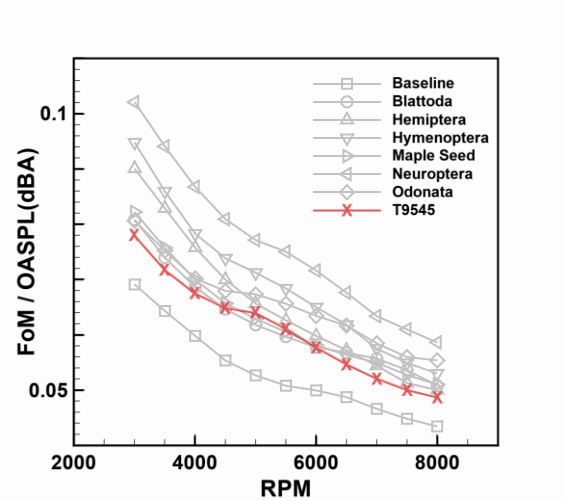

(g) Aeroacoustic effect of bioinspired and T9545 propellers comparison in RPM

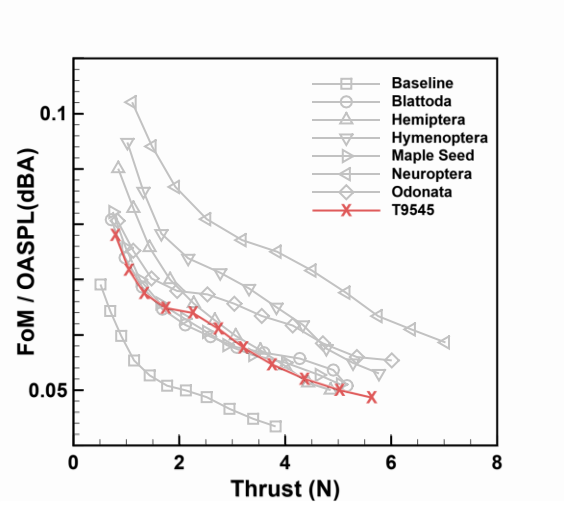

(h) Aeroacoustic effect of bioinspired and T9545 propellers comparison in Thrust

Fig. 10 Aerodynamic, Acoustic, and Aeroacoustic performance results of bioinspired propellers compared to the T9545 propeller at microphone number five

Table 1 Local chord-based Reynolds and Mach numbers of all propellers

Propeller		r/R \ RPM	0.1	0.2	0.3	0.4	0.5	0.6	0.7	0.8	0.9	1
-	Ma	3000	0.01	0.02	0.03	0.04	0.05	0.07	0.08	0.09	0.10	0.11
-		8000	0.03	0.06	0.09	0.12	0.15	0.18	0.21	0.23	0.26	0.29
Baseline	Re	3000	5431	15113	21676	26269	29482	31493	32200	31524	29162	24962
Blattodea		3000	6100	13856	21558	27586	33382	38767	43463	44378	38423	11194
Hemiptera		3000	4196	9980	17399	26765	35594	40667	41384	37355	28790	9305
Hymenoptera		3000	4063	9371	16208	24614	35492	44560	46802	44043	34658	9937
Maple Seed		3000	4185	9996	17936	27758	37382	42203	41879	37235	27715	10306
Neuroptera		3000	4210	10136	17534	26073	35932	45405	52425	53122	45101	8557
Odonata		3000	4669	11012	18127	26132	34110	40566	45379	46809	39600	8709
Baseline		8000	14482	40300	57803	70051	78618	83980	85868	84064	77764	66566
Blattodea		8000	16265	36949	57488	73561	89018	103380	115901	118342	102462	29850
Hemiptera		8000	11189	26614	46397	71373	94917	108446	110356	99612	76774	24814
Hymenoptera		8000	10836	24988	43222	65636	94645	118828	124804	117447	92421	26497
Maple Seed		8000	11159	26656	47828	74021	99685	112542	111676	99292	73908	27482
Neuroptera		8000	11226	27030	46757	69528	95818	121080	139800	141658	120268	22819
Odonata		8000	12452	29366	48340	69686	90959	108177	121010	124825	105601	23224